Materials
Views

www.MaterialsViews.com

ADVANCED
FUNCTIONAL
MATERIALS
www.afm-journal.de

FULL PAPER

Stretchable, Transparent Zinc Oxide Thin Film Transistors

By *Kyungyea Park, Deok-Kyou Lee, Byung-Sung Kim, Haseok Jeon, Nae-Eung Lee, Dongmok Whang, Hoo-Jeong Lee, Youn Jea Kim,* and *Jong-Hyun Ahn**

Stretchable and transparent thin film transistors (TFTs) with intrisically brittle oxide semiconductors are built using a wavy structural configuration that can provide high flexibility and stretchability. After device fabrication procedures including high temperature annealing, the oxide semiconductor-based TFT arrays can be transferred directly to plastic or rubber substrates, without an additional device process, using transfer printing methods. This procedure can avoid some of the thermal degradation problems associated with plastic or rubber substrates by separating them from the annealing procedure needed to improve the device performance. These design and fabrication methods offer the possibility of developing a new format of stretchable electronics.

1. Introduction

Transparent thin film transistors (TTFTs) that offer mechanical stretchability can enable new applications, such as electronic eye imagers on a hemispherical surface and see-through canopy window displays, which require extremely high levels of bendability and fully elastic responses to large strain deformations.[1–3] The key challenge is the design of a system that can enable much higher levels of strain (>>1%) to be tolerated by conventional metal or inorganic materials without fracture or significant degradations in their electronic properties.[3–5] Currently, a representative example of transparent TFTs uses

thin films of inorganic oxides as the semiconducting and conducting layers. Oxide semiconducting materials, such as zinc oxide (ZnO) and indium gallium zinc oxide (IGZO), and oxide conducting materials, such as indium tin oxide (ITO), have a real and potential advantage over silicon-based TFTs in terms of the efficient use of backlight in LCDs or emitted light in OLEDs, as well as high voltage, temperature and radiation tolerance.[6–10] However, these materials have intrinsic limitations in mechanical properties, even though their electrical and optical properties can be good. For example, the tensile fracture strain of ZnO and ITO thin films are less than 0.03% and 1%, respectively.[11,12] Therefore, a significant challenge is to fabricate stretchable TTFTs using oxide materials. This paper proposes to solve this problem using a strain-induced wavy geometry in ZnO-based TTFTs.[13,14] These layouts accommodate a large applied strain without fracturing the materials through changes in the height and wavelength of the wavy structures. As a result, brittle materials, such as ZnO and ITO, can offer effective end-to-end stretchability.

2. Results and Discussion

Figure 1a shows a schematic diagram of the steps for fabricating an array of ZnO TTFTs. The process to achieve this stretchable wavy structure using inorganic oxide materials begins with the fabrication of an array of ZnO TTFTs on a carrier substrate coated with Ge and SiO_2 as sacrificial and protection layers, respectively. For oxidation of as-deposited Ge film, Ge is annealed at over 400 °C because it can be dissolved in water as an oxide.[15,16] The devices are coated with a protective layer of epoxy (~ 1 μm) to position the device layers near the neutral mechanical plane (NMP), where there is zero strain. The location of the NMP in the ZnO device layers, which is weakest against an applied strain, facilitates non-destructive bending of the devices (the bottom image of Figure 1a).[17] Next, reactive ion etching through a patterned layer of photo resist removes certain regions of the epoxy/SiO_2/Ge to isolate the active device islands connected mechanically by thin bridges. The thin device array can then be lifted from the carrier substrate by removing the underlying Ge layer with water. The released thin device film can be transfer-printed again onto a pre-strained elastomeric substrate. Relaxing the pre-strain (ε_{pre}) leads to compressive strain that forms wavy configurations in thin bridges and device regions.[18] The wavelengths and heights

[*] Prof. J.-H. Ahn
School of Advanced Materials Science and Engineering
SKKU Advanced Institute of Nanotechnology
Center for Human Interface Nanotechnology
Sungkyunkwan University
Suwon, 440-476, Korea
E-mail: ahnj@skku.edu
K. Park, B.-S. Kim, Prof. N.-E. Lee, Prof. D. Whang
School of Advanced Materials Science and Engineering
SKKU Advanced Institute of Nanotechnology
Center for Human Interface Nanotechnology
Sungkyunkwan University
Suwon, 440-476, Korea
H. Jeon, Prof. H.-J. Lee
School of Advanced Materials Science and Engineering
Sungkyunkwan University
Suwon, 440-476, Korea
D.-K. Lee, Prof. Y. J. Kim
School of Mechanical Engineering
Sungkyunkwan University
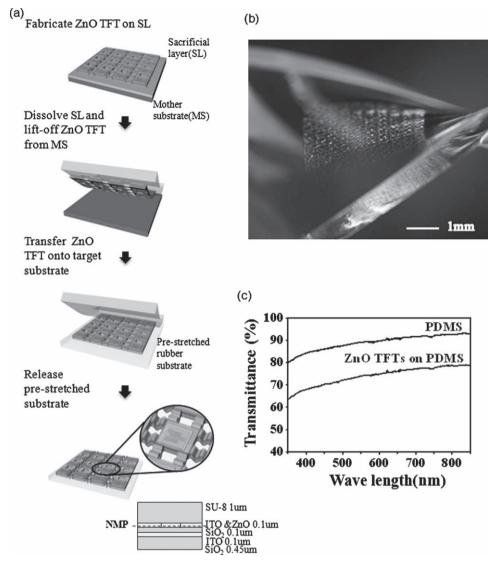Suwon, 440-476, Korea

FULL PAPER

Figure 1. a) Schematic diagram of the method for fabricating stretchable ZnO TFTs to form wavy patterns on a 5% prestrained rubber substrate and an illustration of the position of the neutral mechanical plane. b) Optical micrograph of stretchable, transparent devices on a twisted PDMS substrate. c) Optical transmittance of PDMS substrate and ZnO TFTs on PDMS.

are determined primarily by the thickness of the device layers as well as the elastic properties of the device layers and PDMS. The bottom SiO$_2$ is bonded uniformly to the PDMS surface by covalent –O–Si–O– bonds between the silanol (Si–OH) groups on the PDMS and silicon oxide. Such silanol groups on the top surface of PDMS can be formed through UV/ozone exposure for the surface activation of PDMS. In this format, the system can be stretched uniaxially or isotropically or compressed to high levels of strain (up to 5%). Figure 1b shows an optical image of the transparent, stretchable ZnO device arrays on a PDMS substrate with a thickness of 0.6 mm and a prestrain of 5%. The average transmittance of the ZnO device, exclusive of the PDMS effect region, is approximately 85% for wavelengths between 400 and 800 nm (Figure 1c).

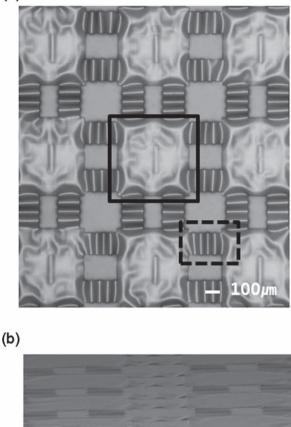**Figure 2a** and b show optical and SEM images of the wavy ZnO TFT arrays on a rubber substrate formed with biaxial

ε_{pre} = 5%. The rectangular island regions of active devices are connected by structural bridges with the wavy patterns induced by releasing the substrate. After releasing the PDMS, most of the wavy patterns occur on thin bridges and wrinkles slightly on thick, rigid device islands, particularly on an area near the bridges.

To determine the effect of these waves or wrinkles on the device, a theoretical simulation was performed by analytical treatments and the finite elements method (FEM). In structural analysis of an island region, the values of stress, strain and deformation by biaxial shrinkage were obtained from the results of a numerical study. The loaded force to each contact boundary between the island part and bridges is approximately −5.5 GPa, when the shrinking phenomenon of the substrate is finished in a stationary solving condition (**Figure 3a**). The thermally induced loads are given by the following equations:[19]

Materials
Views
www.MaterialsViews.com

ADVANCED
FUNCTIONAL
MATERIALS
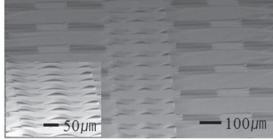www.afm-journal.de

FULL PAPER

Figure 2. a) Magnified optical image of stretchable devices consisting of islands (solid line) that the devices were located on and bridges for connections between islands in a "wavy" pattern (dashed line). b) SEM image of the ZnO TFT with a wavy pattern on bridge and flat region on pad.
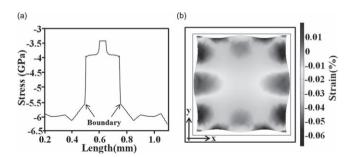

Figure 3. a) Graph of the theoretical loaded force at each contact boundary from island to bridge when shrinking of the PDMS substrate occurs at a stationary solving condition. b) Theoretical two-dimensional finite element simulation of strain as a function of the length in the x-directional.

$$\sigma = D\varepsilon_{el} + \sigma_0 = D(\varepsilon - \varepsilon_{th} - \varepsilon_0) + \sigma_0 \tag{1}$$

$$\varepsilon_{th} = \begin{pmatrix} \varepsilon_x \\ \varepsilon_y \\ \varepsilon_z \\ \gamma_{xy} \\ \gamma_{yz} \\ \gamma_{xz} \end{pmatrix}_{th} = a_{vec}(T - T_{ref}) \tag{2}$$

Here σ, D, α_{vec}, T, T_{ref} denote the stress vector, thermal expansion coefficients, elasticity matrix, actual temperature and reference temperature, respectively. Furthermore, it is assumed that thin film materials forming the device are isotropic and linear elastic using Hooke's law given by[20]

$$\varepsilon_x = \frac{1}{E}\left[\sigma_x - v\left(\sigma_y + \sigma_z\right)\right] \tag{3}$$

$$\varepsilon_y = \frac{1}{E}\left[\sigma_y - v\left(\sigma_z + \sigma_x\right)\right] \tag{4}$$

$$\varepsilon_z = \frac{1}{E}\left[\sigma_z - v\left(\sigma_x + \sigma_y\right)\right] \tag{5}$$

$$\gamma_{xy} = \frac{2(1+v)}{E}\tau_{xy} \tag{6}$$

$$\gamma_{yz} = \frac{2(1+v)}{E}\tau_{yz} \tag{7}$$

$$\gamma_{zx} = \frac{2(1+v)}{E}\tau_{xz} \tag{8}$$

Where σ is the stress vector, ε_x, ε_y, ε_z, γ_{xy}, γ_{yz}, γ_{xz} are the strain components, E is the modulus of elasticity and v is Poisson's ratio. Figure 3b shows the two-dimensional normal strain along the x-direction for the device island. All areas of the island experience small strain (<0.06%) as a result of strain relaxation provided by the bridge. The area of the island near the bridges shows the highest strain (around 0.06%). On the other hand, the center region of the island, where the device composed of ZnO and ITO films is located, shows only 0.01% to 0.02%, which is below the failure strain. The wavelengths and heights of the waves on the bridge can change to accommodate the applied strain in a manner that avoids fracture of the constituent materials.[21]

Figure 4a presents the height (H) and wavelength (λ) of wavy patterns from islands to bridges. The H and λ of the waves in the center of the island regions, determined from the profile, were 0.94 and 200 μm, respectively. On the other hand, the H and λ of the waves in the center of the bridges were 7.40 and 112 μm, respectively. The H value agrees well with that predicted (H = 7.33 μm). However, the λ value shows a slight difference compared to that given by theoretical analysis (λ = 160 μm) (Figure 4b). We believe that the simplifications in the simulation model lead to this difference. In the actual system, the formation of a wavy pattern on the devices can be affected by other factors that are not included in the simulation model, such as environmental conditions and surface roughness.
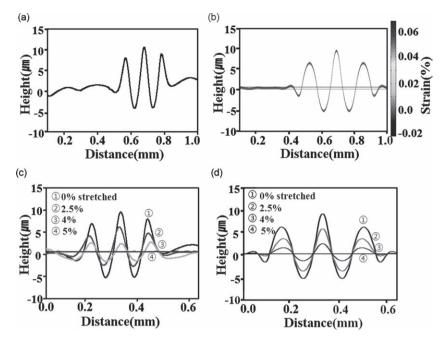
ADVANCED
FUNCTIONAL
MATERIALS
www.afm-journal.de

Materials
Views
www.MaterialsViews.com

FULL PAPER

Figure 4. a) Experimental, and, b) theoretical values of the height and wavelength of the wave on the devices from island to bridge with a pre-strain of 5%. c) Experimental, and, d) theoretical height of bridge at various values of strains (0%, 2.5%, 4%, and 5%).

Figure 4c and d show experimental and theoretical H and λ values of the waves when the device substrates was stretched up to 5%. As they are stretched, the H values of wavy patterns are regularly reduced. When they are stretched up to 5%, wavy patterns are flattened.

Figure 5 shows optical images and electrical measurements of the ZnO TFTs under different tensile, isotropically applied strains for devices fabricated with a 5% pre-strain. The decrease in the heights of the waves of the bridge prevents mechanical failure of the brittle inorganic device components and yields proper functioning under repetitive stretching (Figure 5a). The device before transfer showed an on-off ratio of approximately 10^6, an electron mobility of 1.30 cm^2 V^{-1} s^{-1} and a threshold voltage (V_{th}) of 13 V. After transfer to the rubber substrate, the device exhibited a slight decrease in the on-off ratio (to approximately 10^5) and a change in V_{th} from 13 to 9 V (Figure 5b and c). It is believed that these changes in device properties are caused mainly by degradation of the ZnO/SiO$_2$ interface induced by the water etching process. The OH· radicals from absorbed water can lead to a decrease in the electrical conductivity of ZnO, which results in a threshold voltage shift.[22] In addition, mechanical stress during transfer process can affect the interface between device layers.[23] These kinds of problems may be improved by more careful process optimization. On the other hand, the device after transfer shows no significant change in electrical properties under an applied strain of up to 5%. In addition, the device operates stably, even after hundreds of cycles of compressing/stretching, with electron mobilities of approximately 1.15 ± 0.23 cm^2 V^{-1} s^{-1}(Figure 5d). The small differences between these values suggest that the ZnO TFTs are not damaged by stretching. During mechanical stretching or fatigue testing, most of cracks started to occur in connected parts between island and bridge due to the stress concentration. We believe that this type of failure can be solved through the special design of connected parts, such as a round shape.

Figure 6 shows an optical image of the uniaxial stretching test on ZnO devices. With stretching up to 5%, the waves of bridges along the x-direction were progressively flattened, whereas the wavelength and height of the waves along the y-direction decrease and increase, respectively, due to a Poisson effect, without significant deformation on the islands.[14] This behavior was also observed in the y-directional stretching test (Figure 6c). The electrical measurements of these devices show stable responses under these stretching conditions. The on-off ratios showed little variation immediately after initial stretching along the x- and y- directions but were recovered
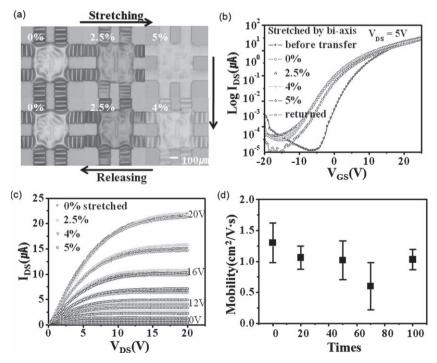

Figure 5. Optical images and electrical measurements of the isotropically stretched TFT on PDMS. a) Optical image of ZnO TFTs shows the configuration of the devices stretched by different strain values of 0%, 2.5%, 4% and 5%. b) Transfer curve, and, c) IV curve under different strain values. d) Plot of the cycling test as a function of the field-effect mobility when the devices are stretched isotropically up to 5% 100 times.

www.MaterialsViews.com

ADVANCED
FUNCTIONAL
MATERIALS
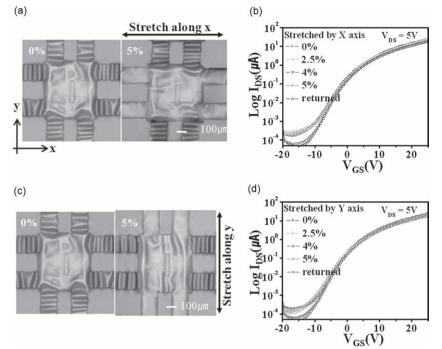www.afm-journal.de

FULL PAPER

Figure 6. Optical images and electrical measurements of the uniaxially stretched TFTs on a PDMS substrate (a and c). Optical image of the released ZnO TFTs (left) and mechanically stretched out (right) in the *x*-direction (5%) (a) and in the *y*-direction (c). b and d) Transfer curve of the stretchable devices in the horizontal (b) and vertical direction (d).

almost perfectly after release, exhibiting good mechanical stability in high strain for stretchable electronics.

3. Conclusions

Stretchable and transparent TFTs with intrisically brittle oxide semiconductors were fabricated using a wavy structural configuration that can provide high flexibility and stretchability. After device fabrication procedures, including high temperature annealing, the oxide semiconductor-based TFT arrays can be transferred directly to plastic or rubber substrates without an additional device process using transfer printing methods. This procedure can avoid some of the thermal degradation problems of plastic or rubber substrates by separating the annealing procedure needed to improve the device performance. These design and fabrication methods offer the possibility of developing a new format of stretchable electronics.

4. Experimental Section

Device Fabrication: To fabricate the transparent thin film transistor, zinc oxide (ZnO), silicon dioxide (SiO_2) and indium tin oxide (ITO) were used as the active layer, insulator, and electrode, respectively. A 300 nm thick germanium (Ge) sacrificial layer and a SiO_2 buffer layer were deposited onto the silicon mother substrate by *e*-beam evaporation. After thermal oxidation at 450 °C for 1 h, a 100 nm ITO film as gate electrode was deposited on the SiO_2 buffer layers by RF magnetron sputtering (RF power density: 100 W cm^{-2}). A 100 nm SiO_2 insulator layer was then deposited at 250 °C and 90 mtorr using plasma-enhanced chemical vapor deposition (PECVD) equipment. A 100 nm undoped ZnO film with 99.99% purity (LTS chemical Inc.) was sputtered using a RF magnetron sputtering system at room temperature without an oxygen partial pressure at a RF power density of 150 W cm^{-2}. After deposition of the ZnO film, the devices were annealed at 350 °C for 1 h in air in a muffle furnace to enhance the electrical properties, and an ITO layer as the source/drain electrode was deposited at a power density of 100 W cm^{-2}. To protect the device, an encapsulation film (SU-8) was coated onto the top of the device using a spin coater and patterned by lithography process to cover only the islands and bridges. They were revealed by a reactive ion etching (RIE) process because the SiO_2 buffer layer should be exposed to the water etchant. The following etching conditions were used: gas ratio of CHF_3 and O_2 (7:1) with a plasma power density of 25 W cm^{-2}.

Transfer Printing: For the stamp, polydimethylsiloxane (PDMS; Sylgard 184, Dow Corning) was cured in a vacuum oven for 6 h, contained in polystyrene Petri dishes. After casting and fully curing the PDMS, a stamp was made by cutting to convenient dimensions. The PDMS stamp was laminated against the TTFTs with an encapsulation film, and peeled off quickly to move the transistor to the surface of the PDMS stamp. The devices were then attached to the receiver, which was an isotropically pre-strained PDMS substrate that was stretched up to 5% on a hot plate and detached from the substrate slowly. In the case of the receiver, it was cured for only 20 min to put a sticky state to tighten up the bonding force between the device and receiver. After transfer to the pre-stretched substrate, PDMS with the devices was fully baked in an oven for 1 h at 70 °C.

Electrical Measurement: To measure the electrical properties of the stretched devices, TFTs on the PDMS substrate were placed onto a hot chuck with a temperature controller and stretched out isotropically by each of the stretched points. The electrical properties of the uniaxially stretched devices along the *x*- or *y*-directions were also measured using the bending machine.

Finite Element Method (FEM): The numerical model was validated using the commercially available computational package, Comsol Multiphysics. The application modules of 2-D plane strain were used to obtain analytical data of the structural interactions. The wavy patterns and deformation characteristic of a pad was first determined. Each layer of the thin film was modeled as a linear elastic material. **Table 1** lists the material properties of the simulated circuit. The simulated models of an island and the wavy pattern of the bridges were designed for simplicity in a 2-D structure, which assumes that the *z*-component of the strain is zero (the side view), in order to analyze wavy patterns of a bridge between two pads. As the boundary conditions of the wavy pattern, the lower left and right corners of SiO_2 (buffer layer) were fixed so that rigid-body movement can be assumed. On the other hand, the other layers

Table 1. Material parameters used in numerical study.

Material	Young's modulus [GPa]	Poisson's ratio	Density [g cm^{-3}]
ITO [24]	116	0.35	7.1
ZnO [11,25]	137	0.36	5.6
SiO$_2$ [26]	70	0.17	2.2
PDMS [27]	0.0018	0.48	0.96

except the buffer layer were not fixed in the *x*-direction to assume a free body and a bonded condition because they are affected by the shrinking force of PDMS. The structural characteristics, such as stress, strain and deformation of an island, were then estimated at a compressive stress of −5.5 GPa, which was the previously obtained stress from the wavy patterns between the island and a bridge. Overall, these simulations give insight into the structural characteristics, such as the deformation of wavy patterns and the mechanics behavior of an island.

Acknowledgements

[1] H. C. Ko, M. P. Stoykovich, J. Song, V. Malyarchuk, W. M. Choi, C. J. Yu, J. B. Geddes Iii, J. Xiao, S. Wang, Y. Huang, *Nature* **2008**, *454*, 748.

[2] G. P. Crawford, *Flexible Flat Panel Displays*, Wiley, New York **2005**.

[3] D. H. Kim, J. Xiao, J. Song, Y. Huang, J. A. Rogers, *Adv. Mater.* **2010**, *22*, 2108

[4] D. Y. Khang, H. Jiang, Y. Huang, J. A. Rogers, *Science* **2006**, *311*, 208.

[5] F. Spaepen, *Acta Mater.* **2000**, *48*, 31.

[6] P. F. Carcia, R. S. McLean, M. H. Reilly, G. Nunes Jr, *Appl. Phys. Lett.* **2003**, *82*, 1117.

[7] R. L. Hoffman, B. J. Norris, J. F. Wager, *Appl. Phys. Lett.* **2003**, *82*, 733.

[8] B. I. Hwang, K. Park, H. S. Chun, C. H. An, H. Kim, H. J. Lee, *Appl. Phys. Lett.* **2008**, *93*, 222104.

[9] K. Nomura, H. Ohta, A. Takagi, T. Kamiya, M. Hirano, H. Hosono, *Nature* **2004**, *432*, 488.

[10] Y. Sun, J. A. Rogers, *Adv. Mater.* **2007**, *19*, 1916.

[11] C. W. Ong, D. G. Zong, M. Aravind, C. L. Choy, D. R. Lu, *J. Mater. Res.* **2003**, *18*, 2464.

[12] Z. Chen, B. Cotterell, W. Wang, *Eng. Fract. Mech.* **2002**, *69*, 597.

[13] D. H. Kim, W. M. Choi, J. H. Ahn, H. S. Kim, J. Song, Y. Huang, Z. Liu, C. Lu, C. G. Koh, J. A. Rogers, *Appl. Phys. Lett.* **2008**, *93*, 044102.

[14] D. H. Kim, J. H. Ahn, W. M. Choi, H. S. Kim, T. H. Kim, J. Song, Y. Y. Huang, Z. Liu, C. Lu, J. A. Rogers, *Science* **2008**, *320*, 507.

[15] R. H. Kingston, *J. Appl. Phys.* **1956**, *27*, 101.

[16] C. P. Liu, *Thin Solid Films* **2002**, *415*, 296.

[17] D. H. Kim, J. Song, W. M. Choi, H. S. Kim, R. H. Kim, Z. Liu, Y. Y. Huang, K. C. Hwang, Y. Zhang, J. A. Rogers, *Proc. Natl. Acad. Sci. U. S. A.* **2008**, *105*, 18675.

[18] X. Lu, Y. Xia, *Nat. Nanotechnol.* **2006**, *1*, 163.

[19] A. E. Huespe, A. Cardona, V. Fachinotti, *Comp. Meth. Appl. Mech. Eng.* **2000**, *182*, 439.

[20] A. P. Boresi, R. J. Schmidt, O. M. Sidebottom, *Advanced Mechanics of Materials*, Wiley, New York **1993**.

[21] S. P. Lacour, J. Jones, S. Wagner, T. Li, Z. Suo, *Proc. IEEE* **2005**, *93*, 1459.

[22] G. Sengupta, H. S. Ahluwalia, S. P. Sen, *J. Colloid Interface Sci.* **1979**, *69*, 217.

[23] K. J. Lee, M. A. Meitl, J. H. Ahn, J. A. Rogers, R. G. Nuzzo, V. Kumar, I. Adesida, *J. Appl. Phys.* **2006**, *100*, 124507.

[24] D. G. Neerinck, T. J. Vink, *Thin Solid Films* **1996**, *278*, 12.

[25] I. Ozen, M. A. Gulgun, M. Ozcan, *Key Eng. Mater.* **2004**, *264*, 1225.

[26] M. T. Kim, *Thin Solid Films* **1996**, *283*, 12.

[27] H. Jiang, D. Y. Khang, J. Song, Y. Sun, Y. Huang, J. A. Rogers, *Proc. Natl. Acad. Sci. U.S.A.* **2007**, *104*, 15607.